Improvements for drift-diffusion plasma fluid models with explicit time integration

Jannis Teunissen[1,2,3]

[1]Centrum Wiskunde & Informatica (CWI), P.O. Box 94079, 1090 GB Amsterdam, The Netherlands
[2]Centre for mathematical Plasma Astrophysics, Department of Mathematics, KU Leuven, Celestijnenlaan 200B, B-3001 Leuven, Belgium
[3]State Key Laboratory of Electrical Insulation and Power Equipment, Xi'an Jiaotong University, Xi'an, China

E-mail: `jannis@teunissen.net`

Abstract. Drift-diffusion plasma fluid models are commonly used to simulate electric discharges. Such models can computationally be very efficient if they are combined with explicit time integration. This paper deals with two issues that often arise with such models. First, a high plasma conductivity can severely limit the time step. A fully explicit method to overcome this limitation is presented. This method is compared to the existing semi-implicit method, and it is shown to have several advantages. A second issue is specific to models with the local field approximation. Near strong density and electric field gradients, electrons can diffuse parallel to the field, and unphysically generate ionization. Existing and new approaches to correct this behavior are compared. Details on the implementation of the models and the various approaches are provided.

1. Introduction

Simulations of electric discharges are often performed with plasma fluid models [1, 2, 3]. Such models require that the mean free path of electrons is small compared to characteristic length scales of the discharge, so they typically become more accurate at higher pressures (e.g. 1 bar). This paper specifically considers drift-diffusion (DD) models with the local field approximation (LFA), which are referred to as DD-LFA models. Such models are commonly used to simulate e.g., streamer discharges [4, 5, 6, 7, 8], plasma jets [9, 10] and dielectric barrier discharges [11].

Compared to particle simulations, fluid models are often much more computationally efficient [12]. Only a few densities have to be evolved per grid cell, instead of tens or hundreds of particles. Updating these densities in time is relatively cheap when an *explicit* time integrator is used, with which the state at time $t + \Delta t$ can explicitly be constructed from the previous state(s). The numerical implementation of a DD-LFA model is discussed in section 2.

However, due to the coupling of charged species to the electric field, an explicit time integrator leads to a restriction on the time step $\Delta t \leq \varepsilon_0/\sigma$, where ε_0 is the permittivity of vacuum and σ the plasma conductivity. This restriction is discussed in more detail in section 3. A new explicit approach is introduced, which avoids the time step restriction by limiting the conductivity of the plasma. The new method is compared to the existing semi-implicit method [13, 14, 15] in several test cases.

Near strong electric field and density gradients, the LFA loses (some of) its validity. An unphysical effect that can occur is that electrons diffuse parallel to the electric field into a high-field region, where they generate ionization. This problem is discussed in detail in section 4. Existing and new approaches to correct this behavior are discussed and tested.

For simplicity, the test cases presented in this paper are one-dimensional. However, the issues addressed are particularly relevant for 2D and 3D simulations, which require both high computational efficiency (and thus explicit schemes) and robustness, due to the sharp gradients and the geometrical complexity that can occur.

2. The DD-LFA model

In this section, a simple DD-LFA (drift-diffusion with local field approximation) model is introduced. Detailed discussions of the validity of this model, which are outside the scope of the present paper, can be found in e.g. [12, 16, 17, 18, 19, 20, 21]. A brief summary is given below.

The accuracy of the LFA depends on the time scale of electron energy relaxation (to the local conditions) compared to other time scales of interest. This energy relaxation occurs through electron-neutral collisions, in particular inelastic ones. In molecular gases at e.g. 1 bar, the LFA therefore works better than in a noble gas at low pressure, if other conditions are kept the same. However, even under favorable conditions, the LFA cannot capture certain (non-local) effects, for example due to spatial density gradients or due to spatial or temporal electric field gradients.

On the other hand, an advantage of the LFA is that only a single equation has to be solved for electrons. Perhaps more important is that the electric field strength is a relatively well-behaved parameter for determining transport coefficients: it is non-negative, well-defined everywhere, and there is a direct link to measured or computed transport coefficients in uniform fields.

2.1. Model formulation

The DD-LFA model considered here was chosen to be as simple as possible. Only electrons and a single positive immobile ion species are included

$$\partial_t n_e = -\nabla \cdot \mathbf{\Gamma} + S, \tag{1}$$
$$\partial_t n_p = S,$$

where n_e is the electron density, n_p the positive ion density, $\mathbf{\Gamma}$ the electron flux and S the ionization source term. With the drift-diffusion approximation, $\mathbf{\Gamma}$ is given by a drift and a diffusion component

$$\mathbf{\Gamma} = \mathbf{\Gamma}^{\mathrm{drift}} + \mathbf{\Gamma}^{\mathrm{diff}} = -n_e \mu_e \mathbf{E} - D_e \nabla n_e, \tag{2}$$

where μ_e is the electron mobility, $\mathbf{E}$ the electric field vector and D_e the electron diffusion coefficient. The electron-impact ionization term is

$$S = \bar{\alpha}\mu_e |\mathbf{E}| n_e = \bar{\alpha} |\mathbf{\Gamma}^{\mathrm{drift}}|, \tag{3}$$

where $\bar{\alpha}$ is the effective ionization coefficient (i.e., ionization minus attachment), and $|\mathbf{E}|$ is the norm of the electric field. With the local field approximation,
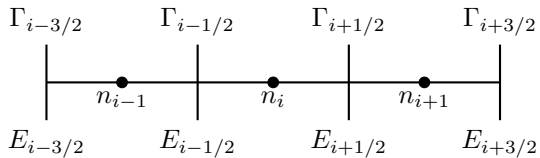
Figure 1. Illustration of a finite-volume discretization in 1D. Densities n_i are stored at cell centers. Fluxes $\Gamma_{i+1/2}$ and electric fields $E_{i+1/2}$ are located at cell faces.

the electron velocity distribution is assumed to be relaxed to the local electric field, so that μ_e, D_e and $\bar{\alpha}$ are functions of $|\boldsymbol{E}|$.

For general (multidimensional) simulations, the electric field is computed from the electrostatic potential ϕ as $\boldsymbol{E} = -\nabla\phi$, and ϕ is obtained by solving a Poisson equation. In simple cases without dielectrics or electrodes, this Poisson equation looks as follows

$$\nabla^2\phi = -\rho/\varepsilon_0, \tag{4}$$

where ε_0 is the permittivity of vacuum, $\rho = (n_p - n_e)e$ the charge density and e the elementary charge. For the 1D simulations considered here, the situation simplifies, as described below.

2.2. Finite volume implementation

Fluid simulations of electric discharges are often performed with finite volume (FV) methods, see e.g. [22, 23]. With a FV method, fluxes are computed at the faces of a cell, and the volume-averaged densities inside a cell are updated with these fluxes, see figure 1.

The flux is here computed using a slope limiter, as described in [24, 25]. The idea behind slope limiters is to interpolate cell-centered densities to the cell faces (where the flux has to be computed) in such a way that numerical errors do not grow in time. The scheme's implementation in 1D is as follows. If $v = -\mu_e E_{i+1/2}$ is the drift velocity at cell face $i + 1/2$, then $\Gamma_{i+1/2}^{\text{drift}}$ is computed as

$$\Gamma_{i+1/2}^{\text{drift}} = \begin{cases} v\left[n_{i+1} - \psi(1/r_{i+1})(n_{i+1} - n_i)\right] & v < 0 \\ v\left[n_i + \psi(r_i)(n_{i+1} - n_i)\right] & v \geq 0 \end{cases}$$

where $r_i = (n_i - n_{i-1})/(n_{i+1} - n_i)$ and $\psi(x)$ is the limiter function. For brevity of notation, the electron density in cell i is here (and later in the paper) indicated by n_i. Note that if $\psi(x) = 0$, the flux is given by the first-order upwind method. As in [24, 25], the Koren [26] limiter is used, given by

$$\psi(x) = \max\left(0, \min(1, (2 + x)/6, x)\right).$$

The diffusive flux is computed as

$$\Gamma_{i+1/2}^{\text{diff}} = -D_e(n_{i+1} - n_i)/\Delta x,$$

where Δx is the grid spacing. Note that with the LFA, μ_e and D_e depend on $|\boldsymbol{E}|$ at the cell face. In 1D, one

can simply take the absolute value, but in multiple dimensions this requires some type of interpolation for the extra components, see e.g. [25].

Unless specified otherwise, source terms are evaluated at the cell centers. Equation (3) is then implemented as

$$S_i = \bar{\alpha}\mu_e|E_i|n_i, \tag{5}$$

where $\bar{\alpha}$ and μ_e depend on the electric field strength at the cell center $|E_i|$, which is here computed as $|E_i| = |E_{i-1/2} + E_{i+1/2}|/2$. As will be shown in sections 3 and 4, it is sometimes beneficial to evaluate the source term at cell faces using the electron flux. On a grid with square cells (e.g., $\Delta x = \Delta y$), equation (3) can then be implemented as

$$S_i = 1/N \sum \bar{\alpha}_{\text{face}}|\Gamma_{\text{face}}^{\text{drift}}|, \tag{6}$$

where the sum runs over all N cell faces, $\bar{\alpha}_{\text{face}}$ depends on the electric field at the cell face, and $\Gamma_{\text{face}}^{\text{drift}}$ is the drift flux through the cell face.

Time integration is here performed with the explicit trapezoidal rule, as in [24, 25]. If equation (1) is written as $\mathbf{y}'(t) = \mathbf{f}(\mathbf{y})$, then this scheme is given by

$$\tilde{\mathbf{y}}_{t+1} = \mathbf{y}_t + \Delta t\,\mathbf{f}(\mathbf{y}_t)$$
$$\mathbf{y}_{t+1} = \mathbf{y}_t + \frac{\Delta t}{2}\left[\mathbf{f}(\mathbf{y}_t) + \mathbf{f}(\tilde{\mathbf{y}}_{t+1})\right].$$

Note that this is an *explicit* scheme, i.e., that $\mathbf{y}_{t+1}$ can explicitly be computed from $\mathbf{y}_t$. Additionally, the classic fourth-order Runge-Kutta time integrator (RK4) is used for some of the convergence tests in section 3. For most of the tests performed here, the time step Δt is fixed. In other cases, it is determined as

$$\Delta t = 0.9 \times \min\left(0.5\,\tau_{\text{CFL}}, \frac{1}{1/\tau_{\text{CFL}} + 1/\tau_{\text{D}}}\right), \tag{7}$$

where τ_{CFL} and τ_{D} are given by the minimum values of $\Delta x/v$ and $\Delta x^2/(2D_e)$, respectively. Another time step restriction related to the plasma conductivity is sometimes required, see section 3 and specifically equation (13).

A new electric field is computed after each (sub)step of the time integrator. In 1D, this is done by starting from a guess for the electric field at the boundary of the domain. The electric fields at all other cell faces can then be obtained from

$$E_{i+1/2} = E_{i-1/2} + \Delta x\,\rho_i/\varepsilon_0,$$

after which the total voltage difference over the domain is determined. Finally, a constant background field is added to ensure the voltage difference becomes the desired applied voltage.

3. The dielectric relaxation time

In a plasma, the movement of charged species is tightly coupled to the electric field. In general, charges move to screen electric fields that are present within the plasma. A characteristic time scale for this screening is the dielectric relaxation time, also known as the Maxwell time [27, 28]

$$\tau = \varepsilon_0/\sigma, \tag{8}$$

where σ is the plasma conductivity. For the discharges considered here, the conductivity is given by

$$\sigma = e \sum_k \mu_k n_k,$$

where μ_k and n_k are the species mobilities and densities. Typically, the contribution of the electron mobility μ_e dominates, so that $\sigma \approx e\mu_e n_e$. In section 3.1, it is shown that for plasma models with explicit time integration, a time step restriction $\Delta t \leq \varepsilon_0/\sigma$ is required.

3.1. Derivation

Equation (8) is derived along the lines of [28]. First, recall Maxwell-Ampère's equation

$$\nabla \times \boldsymbol{B} = \mu_0(\boldsymbol{J} + \varepsilon_0 \partial_t \boldsymbol{E}), \tag{9}$$

where $\boldsymbol{B}$ is the magnetic field, μ_0 the permeability of free space and $\boldsymbol{J}$ the electric current density. Since the divergence of a curl is zero, it follows that

$$\nabla \cdot (\boldsymbol{J} + \varepsilon_0 \partial_t \boldsymbol{E}) = 0. \tag{10}$$

In the electrostatic approximation with $\boldsymbol{B} = 0$ it can be assumed that $\boldsymbol{J}$ and $\boldsymbol{E}$ are (anti-)parallel, since the drift flux is generally (anti-)parallel to $\boldsymbol{E}$ and since the same typically holds for the diffusive fluxes. The divergence can then be transformed into a single spatial derivative, and the generic solution of equation (10) is

$$\partial_t E = -J/\varepsilon_0 + C, \tag{11}$$

where C depends on changes elsewhere in the system‡. Plugging in $J = \sigma E + J^{\text{diff}}$, where J^{diff} are diffusive terms that do not depend on E, gives

$$\partial_t E = -\frac{\sigma}{\varepsilon_0} E - J^{\text{diff}}/\varepsilon_0 + C. \tag{12}$$

When systems with the dynamics of equation (12) are numerically integrated with an explicit method, it is typically required that

$$\Delta t \leq \varepsilon_0/\sigma, \tag{13}$$

otherwise errors grow in time. A physical interpretation of this restriction is that for larger time steps the electric field can reverse, and even be amplified in the reverse direction, which leads to growing errors.

‡ In 1D, $C = 0$ as long as the boundary conditions do not change in time.

3.2. Semi-implicit approach

The time step restriction of equation (13) can be avoided by solving the plasma fluid equations fully implicitly in time. However, obtaining such implicit solutions is usually computationally expensive, in particular in 2D and 3D, which is in part due to the non-linear coupling with the electric field. For this reason, *semi-implicit* discretizations [13, 14, 15] have frequently been used. The idea is to first predict the electric field at $t + \Delta t$ by solving a Poisson equation

$$-\nabla^2 \tilde{\phi} = \nabla \cdot \tilde{\boldsymbol{E}} = \frac{1}{\varepsilon_0} \sum_k q_k \tilde{n}_k, \tag{14}$$

where tildes (˜) indicate estimates at $t + \Delta t$, ϕ is the electric potential, q_k the charge of species k and $\tilde{n}_k$ its density. Since source terms create no net charge, densities can predicted using only the flux Γ, see equation (2):

$$\tilde{n}_k = n_k^t + \Delta t \, \nabla \cdot \boldsymbol{\Gamma}_k(n_k^t, \mu_k^t, D_k^t, \tilde{\boldsymbol{E}}), \tag{15}$$

where the superscript t indicates quantities known at the present time. Combining equations (15), (14) and (2) leads to a variable-coefficient elliptic PDE, which can be solved to obtain $\tilde{\phi}$ and $\tilde{\boldsymbol{E}}$. Afterwards, the fluid equations can be solved using $\tilde{\boldsymbol{E}}$. Such a semi-implicit approach has the following properties:

- The time step restriction of equation (13) is avoided.
- The scheme is first order accurate in time.
- The resulting variable-coefficient elliptic PDE can be solved quite efficiently, but the cost is typically higher than for constant-coefficient cases such as equation (4).

3.3. Current-limited approach

Instead of solving equations implicitly or imposing a restriction on the time step Δt, another option is to limit the conductivity to allow for a larger time step. Equation (13) then becomes

$$\sigma \leq \varepsilon_0/\Delta t. \tag{16}$$

If both sides are multiplied with $|E_j|$, where E_j is the jth component of the electric field, and it is assumed that $\sigma \approx e\mu_e n_e$, equation (16) can be rewritten as

$$\mu_e |E_j| n_e \leq \varepsilon_0 |E_j|/(e\Delta t). \tag{17}$$

The left-hand side of equation (17) is equal to $|\Gamma_j^{\text{drift}}|$, where Γ_j^{drift} is the jth component of the electron drift flux, see equation (2). Instead of limiting only the drift component, it is often preferable to limit the *total* electron flux $|\Gamma_j| = |\Gamma_j^{\text{drift}} + \Gamma_j^{\text{diff}}|$, because diffusive fluxes can also be large near strong density gradients. This is here done according to the following expression

$$|\Gamma_j| \leq \varepsilon_0 E^*/(e\Delta t), \tag{18}$$

where E^* should also take diffusion into account. If diffusion is dominant, electron drift and diffusive fluxes will quickly balance each other, and a reasonable choice for E^* is the electric field at which this occurs. Solving equation (2) for $|\Gamma_j| = 0$ gives $|E_j| = D_e|\partial_j n_e|/(n_e \mu_e)$, where ∂_j is the derivative in direction i. Conversely, if the drift flux is dominant, E^* should be set to $|E_j|$, as was done above. As a general expression for E^*, the maximum of these two cases is used

$$E^* = \max\left(|E_j|, \frac{D_e|\partial_j n_e|}{\mu_e n_e}\right). \tag{19}$$

A robust way to compute $|\partial_j n_e|/n_e$ at the face between cells i and $i+1$, where the flux is defined in finite volume schemes, is

$$\frac{|\partial_j n_e|}{n_e} \approx \frac{|n_{i+1} - n_i|/\Delta x}{\max(n_i, n_{i+1}, \epsilon)}, \tag{20}$$

where Δx is the grid spacing and ϵ is a small number to avoid division by zero. Note that the other quantities in equation (19) can simply be reused from the normal flux computation.

3.3.1. Implementation For convenience, the implementation of the suggested scheme in a discharge model is summarized below:

(i) Determine a time step Δt without taking the dielectric relaxation time $\tau = \varepsilon_0/\sigma$ into account, for example as in equation (7).

(ii) Compute all the components of the electron flux Γ_j at the cell faces between the grid cells, for example as described in section 2.2.

(iii) Compute the values of E^* at the cell faces, using equations (19) and (20).

(iv) Limit the components of the electron flux Γ_j so that equation (18) holds. In other words, if $|\Gamma_j| > \varepsilon_0 E^*/(e\Delta t)$, set $\Gamma_j = \text{sgn}(\Gamma_j)\,\varepsilon_0 E^*/(e\Delta t)$, where $\text{sgn}(x)$ is the sign function.

Sometimes, it can be important to resolve electric screening accurately in time, for example when a highly conductive plasma region is forming. In such cases, the Δt in step (i) can temporarily be reduced.

3.3.2. Discussion The current-limited approach limits the transported charge between two adjacent grid cells within a single time step. Per unit area, the transported charge is $\delta_\sigma = e\,\Delta t\,|\Gamma_j|$, where Γ_j is the electron flux in direction j. From equation (18), it follows that $\delta_\sigma \le \varepsilon_0 E^*$, which corresponds to a change in local electric field satisfying $|\delta_E| \le E^*$. Two cases can be distinguished for E^*, see equation (19). When $E^* = |E_j|$, it follows that the previous field is at most completely screened. When $E^* = D_e|\partial_j n_e|/(\mu_e n_e)$, the change in field is limited by the field that would balance drift and diffusive fluxes.

The current-limited scheme can be applied to drift-diffusion models in general, regardless of whether they use the local field approximation. Advantages of the scheme are that:

- The time step restriction of equation (13) is avoided.

- For time steps fulfilling equation (13) the original behavior of a fluid model is restored.

- It requires only a minor modification of the flux computation.

- The computational cost is low, as the scheme is fully explicit.

3.4. Comparison of current-limited and semi-implicit approach

The current-limited approach is now compared with the semi-implicit method in a simplified 1D test case. Equations (1–2) are solved with the source term set to zero and constant transport coefficients $\mu_e = 0.03\,\text{m}^2/(\text{V}\,\text{s})$ and $D_e = 0.1\,\text{m}^2/\text{s}$. A computational domain of $10\,\text{mm}$ is used, with a grid spacing $\Delta x = 20\,\mu\text{m}$. The right boundary is grounded, and a voltage of $10\,\text{kV}$ is applied at the left boundary. The initial densities n_e and n_p are $10^{20}\,\text{m}^{-3}$ for $4\,\text{mm} \le x \le 6\,\text{mm}$, and zero elsewhere. With these parameters, the dielectric relaxation time of equation (13) becomes $\tau \approx 18.4\,\text{ps}$.

Figure 2 shows the electric field and the electron density at $t = 50\,\text{ns}$ for the current-limited and semi-implicit approach using a time step $\Delta t = 80\,\text{ps}$. For comparison, a reference solution computed with the fourth-order RK4 time integrator and a small time step $\Delta t = 0.1\,\text{ps}$ is also shown. This reference solution was computed on the same grid, without special treatment for the dielectric relaxation time. The current-limited approach agrees very well with the reference solution, whereas the semi-implicit method predicts larger peaks in the electric field at the boundaries of the initially ionized area. The left side of the electron density profile also has a visibly different shape with the semi-implicit approach.

Figure 3 shows the root-mean-square error in the electric field (compared to the reference solution) versus the time step. When the time step is reduced, both the current-limited and the semi-implicit approach appear to converge to the reference solution, although with quite different convergence rates. The semi-implicit method shows roughly first-order convergence. Errors are significantly larger than with the current-limited approach, also for time steps larger than the dielectric relaxation time τ, indicated by the vertical dashed line.

For the current-limited method, the order of convergence depends on the time integrator for
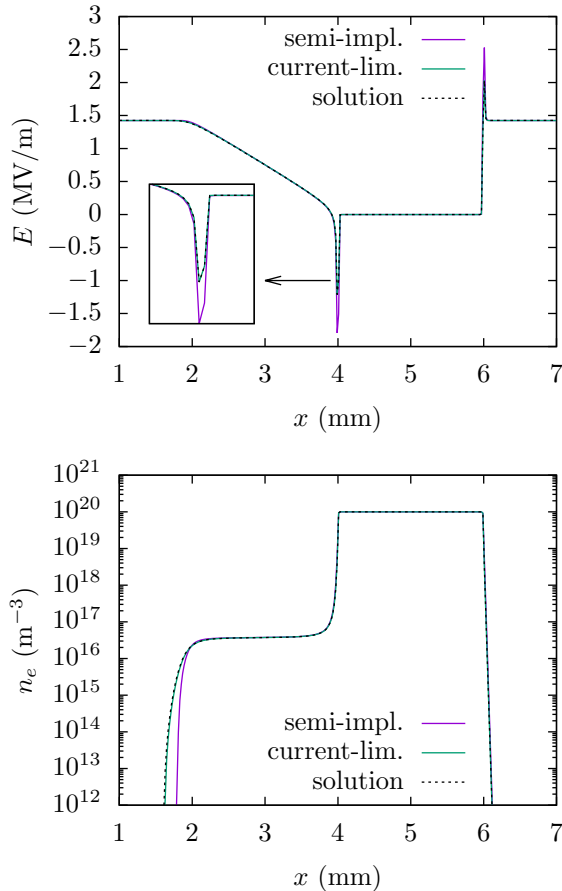
Figure 2. Comparison of the semi-implicit approach with the new current-limited approach. Shown are the electric field (top) and the electron density (bottom) at $t = 50\,\mathrm{ns}$ for the test case described in section 3.4. For both approaches, a time step $\Delta t = 80\,\mathrm{ps}$ is used. A reference solution with a small time step is also shown. With the semi-implicit approach, the electric field has larger peaks at the boundary of the high-density region.

sufficiently small time steps. Two cases are shown: one with the second-order time integrator described in section 2.2, and one with a fourth-order accurate time integrator (RK4). For the latter method, the error saturates for the smallest time steps, which is probably due to numerical round-off errors. For time steps larger than τ, the second and fourth order scheme behave similarly, which indicates that the limiting procedure is the main source of errors.

3.5. Test in nitrogen

In this section, the current-limited approach is used in a more realistic test case in nitrogen at $1\,\mathrm{bar}$ and $300\,\mathrm{K}$. Transport coefficients and the ionization source term are computed with Bolsig+ [29] as function of the applied electric field, using Phelps' cross sections [30]. The same initial condition and grid are used as in section 3.4, but with an applied voltage of $40\,\mathrm{kV}$. After
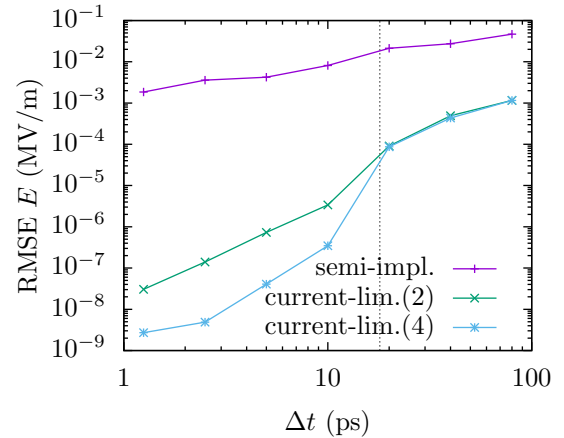
Figure 3. A comparison of the convergence behavior of the semi-implicit and current-limited approaches for the test case described in section 3.4. Shown is the root-mean-square error (compared to the reference solution) in the electric field at $t = 50\,\mathrm{ns}$ versus the time step. For the current-limited approach, results are shown with a second-order and a fourth-order accurate time integrator, indicated by (2) and (4), respectively. The vertical dashed line indicates the dielectric relaxation time.

electric screening has taken place in the initial plasma region, the dielectric relaxation time is about $\tau \approx 3\,\mathrm{ps}$. This value depends on the highest tabulated electron mobility (for the lowest electric field), which was here $\mu_e \approx 0.186\,\mathrm{m^2/(Vs)}$.

Figure 4 shows the electron density and electric field in the system at several times. The solid lines show results with the current-limited approach and a fixed time step $\Delta t = 20\,\mathrm{ps}$. The dashed lines show a reference solution, computed on the same numerical grid but with a small time step $\Delta t = 0.1\,\mathrm{ps}$ and a fourth-order time integrator (RK4). Visually, the current-limited results are almost identical to the reference solution, indicating that the approach also works well in more realistic test cases. The convergence to the reference solution is shown in figure 5. Second order convergence is obtained, which indicates that the current-limited approach does not affect the convergence of the time integration scheme.

3.6. Relevance for discharge simulations

Avoiding the time step restriction due to the dielectric relaxation time τ is beneficial when τ becomes smaller than other time step constraints, in particular when $\tau < \tau_{\mathrm{CFL}}$, see equation (7). This can for example happen when:

- High-density low-pressure discharges are simulated, which have a high conductivity, see e.g. [13, 14].
- A localized high-density and thus high-conductivity region is present, for example near an electrode or
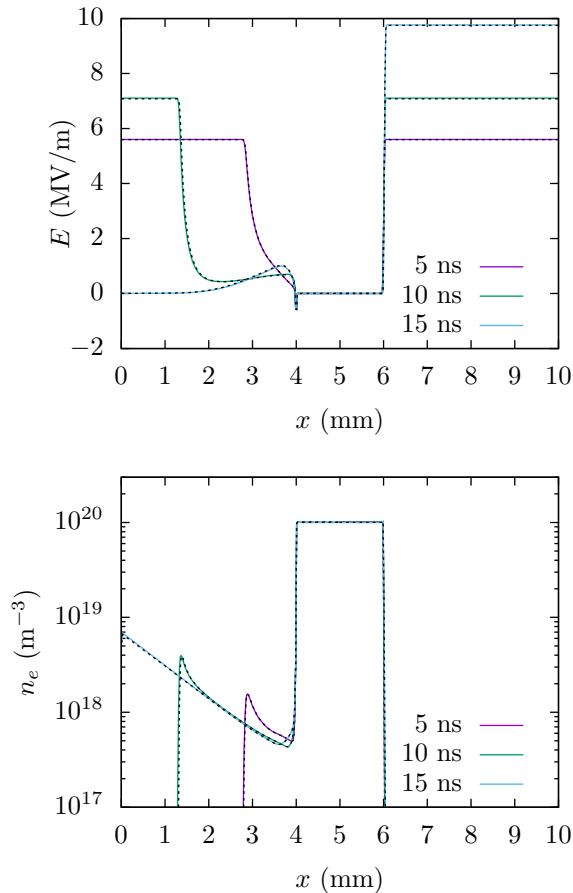
Figure 4. Results of the current-limited approach (solid lines) for a test case in nitrogen, see section 3.5. Shown are the electric field (top) and the electron density (bottom) at several times. The dashed lines indicate a reference solution with a small time step $\Delta t = 20\,\mathrm{ps}$.
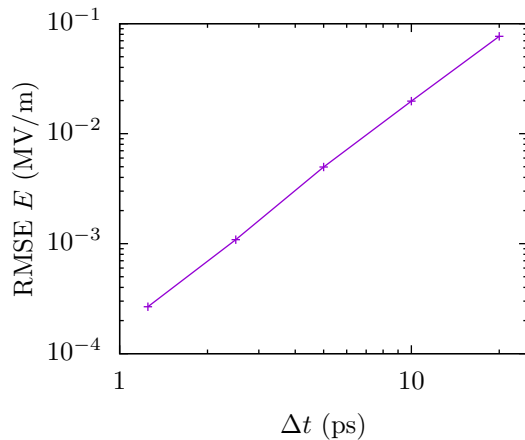
Figure 5. The convergence behavior of the current-limited approach for a test case in nitrogen, see section 3.5. Shown is the root-mean-square error (compared to the reference solution) in the electric field at $t = 10\,\mathrm{ns}$ versus the time step. The line indicates that second order convergence is obtained.

a dielectric material, see e.g. [31, 32], or when streamer discharges stagnate [33].

- The evolution of a conductive plasma is studied after the voltage has been turned off.

4. Unphysical diffusion

The diffusive term in the electron flux of equation (2) can sometimes lead to unphysical behavior, in particular when the diffusive flux has a component parallel to $\boldsymbol{E}$. This can for example happen when there is an electrically screened region with a high electron density, bordered by a region without electrons where the electric field is above breakdown. In reality, electrons should quickly lose energy as they diffuse parallel to the electric field, so that they are effectively confined. However, a fluid model with the LFA does not capture these dynamics, and allows electrons to diffuse into the high-field region§. These electrons then start generating electron-impact ionization, since their ionization rate only depends on the local electric field.

This unphysical effect can for example occur when simulating streamer discharges close to dielectric surfaces [32, 34, 35]. The author has also encountered it in 3D simulations of branching streamer discharges [25], in which some of the smaller branches stop to grow [33].

Below, the unphysical behavior is first demonstrated in a test case. Several approaches to prevent the unphysical behavior are then discussed, and these approaches are compared in section 4.5.

4.1. Test case

The unphysical behavior due to parallel diffusion is present in the test case of section 3.5, but it is not yet visible at $t = 15\,\mathrm{ns}$ in figure 4. To demonstrate the unphysical effect more clearly, simulations are here performed in a higher background field. A computational domain of $4\,\mathrm{mm}$ is used with a voltage difference of $40\,\mathrm{kV}$, so that the background field of $10\,\mathrm{MV/m}$ points in the $+x$-direction. A grid spacing of $\Delta x = 4\,\mu\mathrm{m}$ is used. Initially, $n_e = n_p = 10^{20}\,\mathrm{m}^{-3}$ in the left half of the domain, and $n_e = n_p = 0$ in the right half of the domain. As in section 3.5, the simulations are performed in nitrogen at $1\,\mathrm{bar}$ and $300\,\mathrm{K}$.

The evolution of the electron density is shown in figure 6, which also includes results with half the grid spacing ($\Delta x = 2\,\mu\mathrm{m}$). In both cases, electrons diffuse to the right of the original plasma boundary. When they enter the high-field region, they generate ionization, extending the plasma to the right. Using a finer grid spacing slows down the unphysical growth of the plasma, but does not prevent it. Not shown here

§ Moreover, a strong parallel electric field will typically give a higher diffusion coefficient with the LFA.
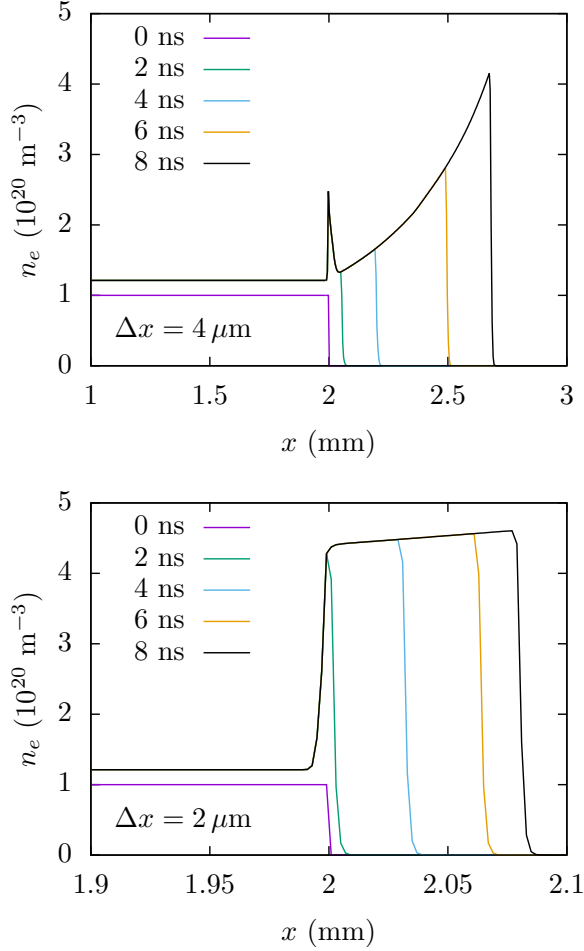
Figure 6. Illustration of the unphysical growth of an ionized region parallel to the electric field, which here points to the right. In the standard DD-LFA model, electrons can diffuse into the high-field region on the right, where they generate impact ionization. The grid spacing for the top and bottom figure are $4\,\mu$m and $2\,\mu$m, respectively.

is the electric field, which is quickly screened in the left half of the domain [28], after which it doubles in the right half of the domain. During the initial electric screening, the degree of ionization in the left half of the domain slightly increases.

4.2. Source term factor (f_ϵ scheme)

The LFA typically becomes less accurate when there are strong density and/or field gradients [36, 37]. Soloviev and Krivtsov [34] derived a correction factor f_ϵ for the impact ionization term from the electron energy equation, which is here referred to as the f_ϵ scheme. This factor can be written as

$$f_\epsilon = 1 - \frac{\hat{E} \cdot \mathbf{\Gamma}^{\text{diff}}}{|\Gamma^{\text{drift}}|} = 1 + \frac{\hat{E} \cdot (D_e \nabla n_e)}{\mu_e n_e |E|}, \qquad (21)$$

where $\hat{E}$ is the electric field unit vector. Near a strong

density gradient such as shown in figure 6, f_ϵ will go to zero, so that no unphysical ionization will take place. This happens because the advective and the diffusive flux balance each other, with the diffusive flux occurring parallel to $\mathbf{E}$. Note that equation (21) also gives reasonable results when the drift and diffusive fluxes do not completely cancel. For example, if the diffusive flux balances half the drift flux ($\mathbf{\Gamma}^{\text{diff}} = -\mathbf{\Gamma}^{\text{drift}}/2$), the result is $f_\epsilon = 1/2$.

A downside of using equation (21) is that the original model formulation is modified, also in regions where there are no unphysical effects due to diffusion. Another issue is how to compute f_ϵ numerically. If the right-most expression of equation (21) is used, there are two problems. First, quantities such as n_e, $\mathbf{E}$ and ∇n_e are not all defined at the same location in a numerical grid cell, so that some type of interpolation or averaging is required. Second, since both n_e and E can be small (or even zero), the division can be problematic. However, f_ϵ can robustly be computed at a cell face if the electron flux is used. In 1D, equation (21) can then be implemented as

$$f_\epsilon = 1 - \frac{\text{sgn}(E)\,\Gamma^{\text{diff}}}{\max(|\Gamma^{\text{drift}}|, \epsilon)}, \qquad (22)$$

where all quantities are defined at the cell face, $\text{sgn}(x)$ is the sign function, and ϵ is a small number to avoid division by zero. In 2D or 3D, the term $\text{sgn}(E)\,\Gamma^{\text{diff}}$ would be replaced by $\hat{E}_j\,\Gamma_j^{\text{diff}}$, where $\hat{E}_j$ is the jth component of the electric field unit vector, and $|\Gamma^{\text{drift}}|$ would be replaced by $|\Gamma_j^{\text{drift}}|$.

When f_ϵ is computed at cell faces, it makes sense to also evaluate the source term at cell faces, so that equation (6) becomes

$$S_i = \left(\bar{\alpha}_L f_{\epsilon,L} |\Gamma_L^{\text{drift}}| + \bar{\alpha}_R f_{\epsilon,R} |\Gamma_R^{\text{drift}}| \right)/2, \qquad (23)$$

where the subscripts L and R indicate values on the left and right face of the cell. In this paper, the f_ϵ scheme is implemented according to equation (23). Alternatively, it is also possible to approximate f_ϵ at the cell center, for example as

$$f_\epsilon = 1 - \frac{\text{sgn}(E_L)\Gamma_L^{\text{diff}} + \text{sgn}(E_R)\Gamma_R^{\text{diff}}}{|\Gamma_L^{\text{drift}}| + |\Gamma_R^{\text{drift}}| + \epsilon},$$

after which the standard source term of equation (5) can be used.

Note that f_ϵ can in principle become negative, which would be unphysical. Here f_ϵ is set to zero in such cases. Similarly, f_ϵ can be restricted to be at most one, to prevent an increase in the source term.

4.3. Source term from flux (FFS scheme)

The source term in equation (3) can also be approximated by the full electron flux

$$S = \bar{\alpha}\mu_e |E| n_e = \bar{\alpha}|\Gamma^{\text{drift}}| \approx \bar{\alpha}|\Gamma|, \qquad (24)$$

where Γ is given by equation (2). This approach is here referred to as the FFS (Full Flux Source) scheme. The FFS scheme has a similar effect as the factor introduced in equation (21). When the advective and diffusive fluxes balance each other, the source term is zero. The effective factor introduced in equation (24) is $g = |\Gamma|/|\Gamma^{\mathrm{drift}}|$. When the advective and diffusive flux are (anti-)parallel, which is always the case in 1D, it follows that $g = f_\epsilon$. For example, when the fluxes are in opposite directions $g = 1 - |\Gamma^{\mathrm{diff}}|/|\Gamma^{\mathrm{drift}}|$, just as for equation (21). In general 2D or 3D cases, $g \neq f_\epsilon$. When the advective and diffusive flux are orthogonal, $g = \sqrt{1 + (|\Gamma^{\mathrm{diff}}|/|\Gamma^{\mathrm{drift}}|)^2}$, whereas $f_\epsilon = 1$. However, in such cases the diffusive flux is typically small compared to the advective flux, so that $g \approx 1 + (|\Gamma^{\mathrm{diff}}|/|\Gamma^{\mathrm{drift}}|)^2/2 \approx 1$.

Compared to equation (21), there is less physical motivation for equation (24). Both approaches have the drawback that the original model formulation is changed. However, numerically equation (24) is easier to implement than equation (21), since the electron flux is readily available. The source term can be computed similar to equation (6), so that in 1D it is given by

$$S = (\bar{\alpha}_L|\Gamma_L| + \bar{\alpha}_R|\Gamma_R|)/2, \tag{25}$$

where Γ_L and Γ_R are the flux through the left and right face of the cell. Finally, note that equation (24) can be modified so that it does not increase the source term by replacing $|\Gamma|$ with $\min(|\Gamma^{\mathrm{drift}}|, |\Gamma|)$.

4.4. Limiting parallel diffusion

With the above two methods, the source term is modified next to a strong density gradient. This prevents electrons that have diffused across the gradient from generating new ionization. Another approach could be to limit diffusion parallel to the electric field, which can be implemented as:

if $\Gamma_j^{\mathrm{diff}} E_j > 0$ and $|E_j| > E_{\mathrm{lim}}$ then set $\Gamma_j^{\mathrm{diff}} = 0$.

Or in words: if the jth component of the diffusive flux points in the same direction as E_j, and if $|E_j|$ exceeds some threshold E_{lim}, set the diffusive flux to zero. By setting E_{lim} to the critical field, above which the net ionization rate is positive, electrons cannot diffuse into a region where they generate ionization.

Advantages of this approach are that only the diffusion equation has to be modified and that the implementation is relatively simple. However, there are also some downsides. As long as the electron density is not strictly zero, ionization continues to occur when the field is above breakdown. For the implementation described above, it is also necessary to evaluate the source term using the electron drift flux, as in equation (6). Otherwise, electrons can diffuse in from one of the
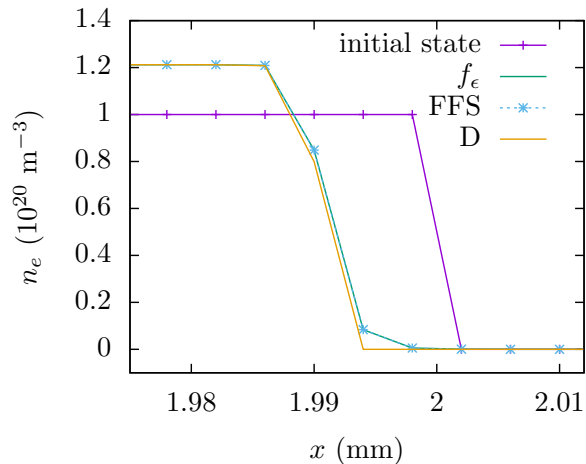
Figure 7. Comparison of methods to address unphysical diffusion, showing the electron density at $t = 8\,\mathrm{ns}$ for the test case described in section 4.1. The f_ϵ curve corresponds to equation (21), the FFS curve to equation (24) and the D curve to the diffusion-limited approach described in section 4.4. The f_ϵ and FFS scheme give identical results. All methods prevent unphysical growth of the discharge to the right.

cell faces (with a low field), and generate ionization at the cell center due to a high field on the other cell face.

4.5. Comparison of the schemes

In figure 7, the effect of the three approaches described above is compared. Applied to the half-ionized domain test case described in section 4.1, the results at $t = 8\,\mathrm{ns}$ show no unphysical propagation to the right. As expected, equation (21) and equation (24) give identical results in 1D. With the diffusion-limited approach, the electron density drops to zero more rapidly. From this 1D test, it cannot be concluded which scheme will perform best for general 2D and 3D cases; this question is left for future work.

In this paper, several approaches have been described for computing the ionization source term. Their effect on a developing discharge is illustrated in figure 8, which shows results for four cases:

- A standard DD-LFA model, using equation (5) as the source term

- A DD-LFA model that uses the drift flux for the source term, see equation (6)

- The ϵ and FFS schemes (which give identical results)

- The ϵ and FFS schemes, modified such that they do not increase the ionization rate

The same computational domain and gas as in section 4.1 are used, but with $30\,\mathrm{kV}$ applied voltage. Initially, $n_e = n_p = 10^{10}\,\mathrm{m}^{-3}$ for $2.95\,\mathrm{mm} \leq x \leq 3.05\,\mathrm{mm}$, and
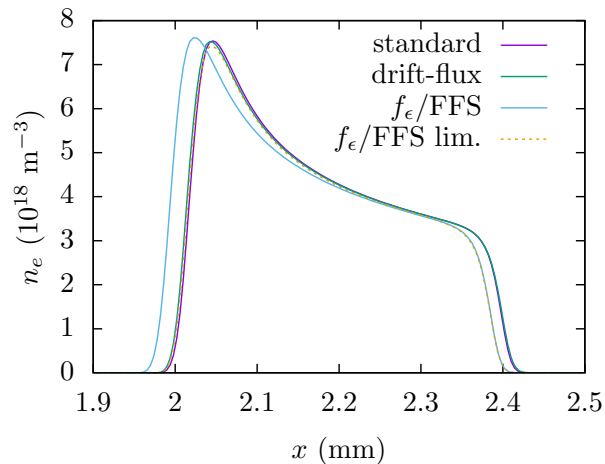
Figure 8. Comparison of several methods to compute the ionization source term for the test case described in section 4.5. The electron density at $t = 3$ ns is shown. Using equation (5) for the source term (labeled *standard*) produces almost the same results as equation (6) (labeled *drift-flux*). The f_ϵ/FFS schemes can increase the source term, which causes the discharge to propagate slightly faster. When the source is limited (so that it does not exceed its 'normal' value) this effect disappears, as indicated by the dashed line.

zero elsewhere. All simulations were performed with a fixed time step $\Delta t = 3$ ps.

With the ϵ/FFS schemes, the source term on the right side of the discharge is reduced, leading to a smaller extension in this direction. Conversely, these schemes increase the source term on the left side, leading to faster leftward propagation than with the standard model. Having a higher ionization rate in front of the discharge physically makes sense [20], but the changes introduced by equations (21) and (24) are not necessarily the best way to correct for this. When the ϵ/FFS schemes are modified so that they do not increase the source term, the results are in good agreement with the standard model for the leftward propagation. Finally, figure 8 shows that equation (5) and equation (6) give almost the same results for this test case.

5. Summary and discussion

The main contributions of the present paper are:

- A new explicit approach to avoid the dielectric relaxation time step restriction was presented in section 3. Compared with the existing semi-implicit method, the new current-limited approach is faster, simpler to implement, does not reduce the order of accuracy of the time integrator, and it reverts to the original model for sufficiently small time steps. The proposed current-limited approach can be used with different types of

plasma fluid models.

- With the local field approximation, unphysical effects can occur when there is diffusion parallel to the electric field. Several methods to avoid this were compared in section 4. An existing approach [34] was compared with two new approaches. All methods could prevent the unphysical effects in 1D.

- Different methods for implementing the ionization source term were described, as well as implementation details for the approaches listed above. General implementation aspects for explicit drift-diffusion fluid models were also discussed.

The methods described here are particularly relevant for the simulation of pulsed discharges near dielectrics and electrodes. Near such boundaries, there can be high electron densities, strong electric fields, and strong spatial gradients in both quantities, see e.g. [32]. For simplicity, tests were here performed in 1D, although the described methods can also be used in 2D and 3D. Performing these 2D and/or 3D tests is an important next step that is left for future work. For the unphysical effects due to diffusion, it would also be interesting to investigate the effect of using an energy equation instead of the local field approximation.

Software availability

The source code of the simulation software used in this paper is available at: `https://gitlab.com/MD-CWI-NL/streamer_1d` and `https://github.com/jannisteunissen/semi_implicit_fluid`.

References

[1] Gogolides E and Sawin H H 1992 *J. Appl. Phys.* **72** 18
[2] Dujko S, Markosyan A H, White R D and Ebert U 2013 *J. Phys. D: Appl. Phys.* **46** 475202 ISSN 1361-6463
[3] Alves L L, Bogaerts A, Guerra V and Turner M M 2018 *Plasma Sources Science and Technology* **27** 023002 ISSN 1361-6595
[4] Luque A and Ebert U 2012 *Journal of Computational Physics* **231** 904–918 ISSN 00219991
[5] Bagheri B, Teunissen J, Ebert U, Becker M M, Chen S, Ducasse O, Eichwald O, Loffhagen D, Luque A, Mihailova D and al e 2018 *Plasma Sources Science and Technology* **27** 095002 ISSN 1361-6595
[6] Marskar R 2019 *Journal of Computational Physics* **388** 624–654 ISSN 00219991

[7] Plewa J M, Eichwald O, Ducasse O, Dessante P, Jacobs C, Renon N and Yousfi M 2018 *Journal of Physics D: Applied Physics* **51** 095206 ISSN 0022-3727, 1361-6463

[8] Komuro A, Matsuyuki S and Ando A 2018 *Plasma Sources Science and Technology* **27** 105001 ISSN 1361-6595

[9] Boeuf J P, Yang L L and Pitchford L C 2013 *Journal of Physics D: Applied Physics* **46** 015201 ISSN 0022-3727, 1361-6463

[10] Bourdon A, Darny T, Pouvesle J M, Viegas P and Is S 2016 *Plasma Sources Sci. Technol.* 18

[11] Stollenwerk L and Amiranashvili S 2006 *PHYSICAL REVIEW LETTERS* 4

[12] Kim H C, Iza F, Yang S S, Radmilovi\'c-Radjenovi\'c M and Lee J K 2005 *Journal of Physics D: Applied Physics* **38** R283–R301 ISSN 1361-6463

[13] Ventzek P L, Hoekstra R J and Kushner M J 1994 *Journal of Vacuum Science & Technology B: Microelectronics and Nanometer Structures Processing, Measurement, and Phenomena* **12** 461–477

[14] Lapenta G, Iinoya F and Brackbill J Aug/1995 *IEEE Transactions on Plasma Science* **23** 769–779 ISSN 00933813

[15] Hagelaar G and Kroesen G 2000 *Journal of Computational Physics* **159** 1–12 ISSN 00219991

[16] Grubert G K, Becker M M and Loffhagen D 2009 *Physical Review E* **80** ISSN 1550-2376

[17] Becker M M and Loffhagen D 2013 *AIP Advances* **3** 012108 ISSN 2158-3226

[18] Markosyan A H, Teunissen J, Dujko S and Ebert U 2015 *Plasma Sources Science and Technology* **24** 065002 ISSN 1361-6595

[19] Eichwald O, Ducasse O, Merbahi N, Yousfi M and Dubois D 2005 *Journal of Physics D: Applied Physics* **39** 99–107 ISSN 1361-6463

[20] Li C, Brok W J M, Ebert U and van der Mullen J J A M 2007 *Journal of Applied Physics* **101** 123305 ISSN 0021-8979

[21] Drallos P J, Nagorny V P and Williamson W 1995 *Plasma Sources Science and Technology* **4** 576–590 ISSN 0963-0252, 1361-6595

[22] LeVeque R J 2002 *Finite Volume Methods for Hyperbolic Problems* Cambridge Texts in Applied Mathematics (Cambridge ; New York: Cambridge University Press) ISBN 978-0-521-81087-6 978-0-521-00924-9

[23] Toro E F 2009 *Riemann Solvers and Numerical Methods for Fluid Dynamics: A Practical Introduction* 3rd ed (Dordrecht ; New York: Springer) ISBN 978-3-540-25202-3 978-3-540-49834-6 oCLC: ocn401321914

[24] Montijn C, Hundsdorfer W and Ebert U 2006 *Journal of Computational Physics* **219** 801–835 ISSN 00219991

[25] Teunissen J and Ebert U 2017 *Journal of Physics D: Applied Physics* **50** 474001 ISSN 1361-6463

[26] Koren B 1993 A robust upwind discretization method for advection, diffusion and source terms *Numerical Methods for Advection-Diffusion Problems* ed Vreugdenhil C B and Koren B (Braunschweig/Wiesbaden: Vieweg) pp 117–138

[27] Barnes M S, Cotler T J and Elta M E 1987 *Journal of Applied Physics* **61** 81 ISSN 0021-8979

[28] Teunissen J, Sun A and Ebert U 2014 *Journal of Physics D: Applied Physics* **47** 365203 ISSN 0022-3727, 1361-6463

[29] Hagelaar G J M and Pitchford L C 2005 *Plasma Sources Science and Technology* **14** 722–733 ISSN 0963-0252, 1361-6595

[30] Phelps A V and Pitchford L C 1985 *Phys. Rev. A* **31** 2932–2949

[31] Teunissen J and Ebert U 2016 *Plasma Sources Science and Technology* **25** 044005 ISSN 1361-6595

[32] Babaeva N Y, Tereshonok D V and Naidis G V 2016 *Plasma Sources Science and Technology* **25** 044008 ISSN 1361-6595

[33] Pancheshnyi S V and Starikovskii A Y 2004 *Plasma Sources Science and Technology* **13** B1–B5 ISSN 0963-0252, 1361-6595

[34] Soloviev V R and Krivtsov V M 2009 *Journal of Physics D: Applied Physics* **42** 125208 ISSN 0022-3727, 1361-6463

[35] Soloviev V and Krivtsov V 2017 *Journal of Physics: Conference Series* **927** 012059 ISSN 1742-6588, 1742-6596

[36] Naidis G V 1997 *Technical Physics Letters* **23** 493–494 ISSN 1090-6533

[37] Li C, Ebert U and Hundsdorfer W 2010 *Journal of Computational Physics* **229** 200–220 ISSN 0021-9991